A Quantum Scanning Microscope for Cold Atoms

D. Yang,[1,2] C. Laflamme,[1,2] D. V. Vasilyev,[1,2] M. A. Baranov,[1,2] and P. Zoller[1,2]

[1]*Institute for Theoretical Physics, University of Innsbruck, A-6020 Innsbruck, Austria*

[2]*Institute for Quantum Optics and Quantum Information of the Austrian Academy of Sciences, A-6020 Innsbruck, Austria*

(Dated: September 7, 2017)

We describe a scanning microscope to monitor 'live' the quantum dynamics of cold atoms in a Cavity QED setup. The microscope measures the atomic density with subwavelength resolution via dispersive couplings to a cavity and homodyne detection within the framework of continuous measurement theory. We analyze two modes of operation. First, for a fixed focal point the microscope records the wave packet dynamics of atoms with time resolution set by the cavity lifetime. Second, a spatial scan of the microscope acts to map out the spatial density of a static system. Remarkably, in the latter case, for a good cavity limit, the microscope becomes an effective quantum non-demolition device, such that the spatial distribution of motional eigenstates can be measured back-action free in single scans.

arXiv:1709.01530v1 [quant-ph] 5 Sep 2017

Spatially resolved observation of individual atoms is a key ingredient in exploring quantum many-body dynamics with ultracold atoms. This is highlighted by the recent development of the quantum gas microscope [1] where fluorescence measurements provide us with single shot images of atoms in optical lattices. Fluorescence imaging is, however, an inherently destructive quantum measurement, as it is based on multiple resonant light scattering resulting in recoil heating. In contrast, quantum motion of cold atoms can also be observed in nondestructive, weak measurements, realizing the paradigm of *continuous measurement* of a quantum system [2–4]. Below we describe and analyze a quantum optical setup for a *scanning atomic microscope* employing dispersive interactions in a Cavity QED (CQED) setup [5], where the goal is to achieve continuous observation of the density of atomic quantum systems [6] with subwavelength resolution [7]. We will be interested in an operating mode, where we perform a spatial scan with the microscope to map out density distributions as a quantum non-demolition (QND) measurement [8]; and in another mode, where we monitor at a fixed position, the time resolved response to 'see' quantum motion of atoms.

The operating principle of the microscope is illustrated as a CQED setup in Fig. 1: We assume that an atom traversing the focal region of the microscope signals its presence with an internal spin flip, i.e. the position, and thus motion of the atom, is correlated with its internal spin degree of freedom. While subwavelength spatial resolution can in principle be achieved by driving transition between spin states in the presence of external fields generating energy shifts with strong spatial gradients [9, 10], this spatial resolution is typically accompanied with strong forces acting on the atom. Instead we will describe below a setup with diminished disturbance, based on *position dependent 'dark state'* in a Λ-system [11], involving a pair of longlived atomic ground state levels, representing the spin. We can detect this spin flip nondestructively with a dispersive interaction, e.g. as shift of a cavity mode of an optical resonator. Thus the atom traversing the focal region of the microscope, as defined by lasers generating the atomic dark
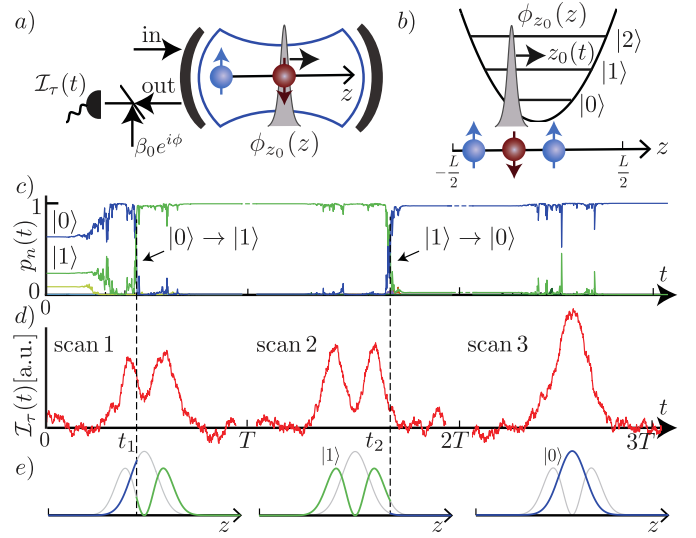

FIG. 1. a) Scanning Microscope as a CQED setup: The atom signals its presence in the focal region with subwavelength resolution as a spin flip, detected via a dispersive cavity coupling in homodyne measurement. (b) *Spatial scan* of the focal point $z_0 = z_0(t)$ for an atom in a harmonic oscillator (HO). c)-e) Operation of the microscope in the good cavity limit as emergent QND measurement (see text). For an atom in a thermal state of the HO we *simulate a single measurement run* involving three consecutive spatial scans: c) conditional trap populations $p_n(t)$ ($n = 0, 1, 2$), and d) homodyne current $\mathcal{I}_\tau(t)$. QND measurement prepares the atom in a trap state $|n\rangle$, and $\mathcal{I}_\tau(t)$ traces the corresponding density e) in the subsequent scan. Times t_1, t_2 indicate quantum jumps between trap states (see text).

state, becomes visible as a phase shift of the laser light reflected from the cavity. This phase shift is revealed in homodyne detection. Such CQED schemes are timely in view of both the recent progress with cold atoms in cavity and nano-photonic setups [12–20], and the growing interests in conditional dynamics of cold atoms under measurement [21–25].

Below we will develop a quantum optical model of con-

tinuous measurement [3, 4, 26] of atomic density, via measurement of the homodyne current for the setup described in Fig. 1. We adopt the language of the Stochastic Master Equation (SME) for the conditional density matrix $\rho_c(t)$ of the joint atom-cavity system, which describes time evolution conditional to observation of a given homodyne current trajectory, as 'seen' in a single run of an experiment, and including the backaction on the atom. This will allow us to address to what extent the observed homodyne current in a spatial scan provides a faithful measurement of atomic density, and the expected signal-to-noise ratio (SNR).

Quantum Optical Model – We consider a model system of an atom moving in 1D along the z-axis, which is placed in a driven optical cavity. To detect the atom at z_0 with resolution σ we introduce a spatially localized dispersive coupling of the atom to a single cavity mode of the form

$$\hat{H}_{\text{coup}} = \phi_{z_0}(\hat{z})\,\hat{c}^\dagger \hat{c}. \tag{1}$$

Here $\phi_{z_0}(z)$ defines a sharply peaked *focusing function* of support σ around z_0, and $\hat{c}^\dagger \hat{c}$ is the photon number operator for the cavity mode with destruction (creation) operators $\hat{c}(\hat{c}^\dagger)$. An implementation of $\phi_{z_0}(\hat{z})$ achieving optical subwavelength resolution $\sigma \ll \lambda$ based on atomic dark states in a Λ-system will be described below. We find it convenient to write $\phi_{z_0}(z) \equiv \mathcal{A}f_{z_0}(z)$ with $f_{z_0}(z)$ normalized, and $\mathcal{A}$ a constant with the dimensions of energy.

According to Eq. (1), the presence of an atom inside the focal region results in a shift of the cavity resonance. This can be detected with a homodyne measurement, where the output field of the cavity is superimposed with a local oscillator with phase ϕ. The homodyne current can, for a single measurement trajectory, be written as $I(t) = \sqrt{\kappa}\langle \hat{X}_\phi \rangle_c + \xi(t)$, i.e. follows the expectation value of the quadrature operator of the intracavity field, $\hat{X}_\phi \equiv e^{i\phi}\hat{c}^\dagger + e^{-i\phi}\hat{c}$, up to the (white) shot noise $\xi(t)$. Here κ represents the cavity damping rate, and $\langle \dots \rangle_c \equiv \text{Tr}\{\dots \rho_c(t)\}$ refers to an expectation value with respect to the conditional density matrix of the joint atom-cavity system.

On a more formal level, we write for the evolution under homodyne detection the Itô stochastic differential equations for the homodyne current

$$dX_\phi(t) \equiv I(t)dt = \sqrt{\kappa}\langle \hat{X}_\phi \rangle_c dt + dW(t), \tag{2}$$

with $dW(t)$ Wiener noise increments, and the SME for a conditional density matrix

$$d\rho_c = -\frac{i}{\hbar}[\hat{H}, \rho_c]dt + \kappa\mathcal{D}[\hat{c}]\rho_c dt + \sqrt{\kappa}\mathcal{H}[\hat{c}e^{-i\phi}]\rho_c dW(t). \tag{3}$$

Eq. (2) identifies the homodyne current as measurement of the quadrature component $dX_\phi(t)$ of the outfield in a time step $[t, t+dt)$. The SME (3) contains the total Hamiltonian $\hat{H} = \hat{H}_{\text{sys}} + \hat{H}_{\text{c}} + \hat{H}_{\text{coup}}$ with $\hat{H}_{\text{sys}} = \hat{p}_z^2/2m + V(\hat{z})$ the Hamiltonian of the atomic system in an external potential V, $\hat{H}_{\text{c}} = i\hbar\sqrt{\kappa}\mathcal{E}(\hat{c} - \hat{c}^\dagger)$ the

Hamiltonian for the driven cavity in the rotating frame (we assume resonant driving for simplicity), and $\mathcal{E}$ the coherent amplitude of the cavity mode driving field. The last two terms in Eq. (3) account for the back-action of the homodyne measurement. The Lindblad operator $\mathcal{D}[\hat{c}]\rho = \hat{c}\rho\hat{c}^\dagger - \frac{1}{2}\hat{c}^\dagger\hat{c}\rho - \frac{1}{2}\rho\hat{c}^\dagger\hat{c}$ describes the system decoherence (the cavity field damping) due to the coupling to the outside electromagnetic modes, and the nonlinear operator $\mathcal{H}[\hat{c}]\rho_c \equiv \hat{c}\rho_c - \langle\hat{c}\rangle_c\rho_c + \text{H.c.}$ updates the density matrix conditioned on the observation of the homodyne photocurrent $I(t)$.

To reveal the relation between the homodyne current and the measurement of local atomic density, we consider the limit where the cavity response time $\tau_c = \hbar/\kappa$ is much faster than other time scales including atomic motion $\hat{H}_{\text{sys}}$, and the dispersive coupling f_{z_0} (the bad cavity limit). Adiabatic elimination of the cavity gives

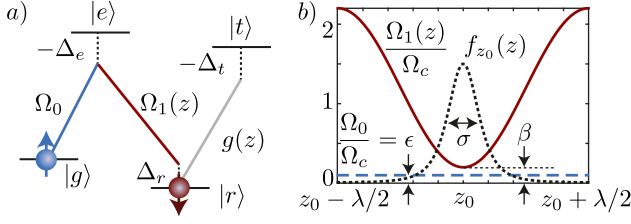$$dX_\phi(t) \equiv I(t)dt = 2\sqrt{\gamma}\langle f_{z_0}(\hat{z})\rangle_c\,dt + dW(t), \tag{4}$$

with the atomic conditional density matrix $\tilde{\rho}_c(t)$ obeying the SME

$$d\tilde{\rho}_c = -\frac{i}{\hbar}[\hat{H}_{\text{sys}}, \tilde{\rho}_c]\,dt + \gamma\mathcal{D}[f_{z_0}(\hat{z})]\tilde{\rho}_c\,dt$$
$$+ \sqrt{\gamma}\mathcal{H}[f_{z_0}(\hat{z})]\tilde{\rho}_c\,dW(t). \tag{5}$$

Here $\gamma = [4\mathcal{A}\mathcal{E}/(\hbar\kappa)]^2$ is an effective coupling rate for the measurement, and we have chosen $\phi = -\pi/2$ (Appendix B). According to Eq. (4) the homodyne current $I(t)$ is a direct probe of the local atomic density at z_0 with spatial resolution σ [27]. Eqs. (4) and (5), or (2) and (3) in the general case, provide us with the tools to study dynamics of the 'microscope' in various modes of operation (see below).

Instead of single trajectories, we can also consider ensemble averages corresponding to repeated preparation and measurement cycles. We define a density operator for the cavity-atom system $\rho(t) = \langle\rho_c(t)\rangle_{\text{st}}$ as statistical average over the conditional density matrices, and an averaged homodyne current $\langle I(t)\rangle_{\text{st}} = \sqrt{\kappa}\text{Tr}\{\hat{X}_\phi\rho(t)\}$. This density operator obeys a master equation (ME), which is obtained from the SME (3) by averaging over trajectories. Thus $\rho_c(t) \to \rho(t)$ in Eq. (3) with the stochastic term dropped according to the Itô property $\langle\dots dW(t)\rangle_{\text{st}} = 0$. An analogous ME for the atom $\tilde{\rho}(t) = \langle\tilde{\rho}_c(t)\rangle_{\text{st}}$ can be derived from the adiabatically eliminated SME (5) (Appendix B).

Implementation of the focusing function $\phi_{z_0}(\hat{z})$ – The atom-cavity coupling Eq. (1) with subwavelength resolution can be achieved using the position-dependent dark state of a Λ-system [11, 28, 29]. We consider the level scheme of Fig. 2a, where two atomic ground (spin) states $|g\rangle$ and $|r\rangle$ are coupled to the excited state $|e\rangle$ with Rabi frequencies Ω_0 and $\Omega_1(z)$, respectively. This configuration supports a dark state $|D(z)\rangle = \sin\theta(z)|g\rangle - \cos\theta(z)|r\rangle$ with $\tan\theta(z) = \Omega_1(z)/\Omega_0$, as superposition of the two atomic ground states, which via destructive interference is decoupled from the dissipative excited state $|e\rangle$.

FIG. 2. Implementing the focusing function $\phi_{z_0}(z)$. a) The Λ-configuration $|g\rangle, |r\rangle, |e\rangle$ supporting a dark state with a sub-wavelength spin structure associated with the ground states (see text), and dispersive cavity coupling on the transition $|r\rangle \rightarrow |t\rangle$. b) The Rabi frequencies, $\Omega_1(z) = \Omega_c\{1 + \beta + \sin[k(z - z_0)]\}$ (solid line), $\Omega_0 = \epsilon\Omega_c$ (dashed line), and the focusing function $f_{z_0}(z)$ (dotted line) shown for $\epsilon = \beta/2 = 0.1$. For this configuration, the corresponding non-adiabatic potential [28, 29] (see Appendix A) is strongly suppressed.

We note that in spatial regions $\Omega_1(z) \gg \Omega_0$ the atom will be (dominantly) in state $|g\rangle$, while in regions $\Omega_1(z) \ll \Omega_0$ the atom will be in $|r\rangle$. This allows us to define via the spatial dependence of $\Omega_1(z)$ regions with subwavelength resolution $|z - z_0| \lesssim \sigma \ll \pi/k = \lambda/2$, characterized by atoms in $|r\rangle$. Atoms in $|r\rangle$ can be dispersively coupled to the cavity mode, resulting in a shift $g^2(z)/\Delta_t\hat{c}^\dagger\hat{c}$, with $g(z)$ the cavity coupling much smaller than the detuning Δ_t (c.f. Fig. 2a). Thus atoms prepared in the dark state experience a shift (1) with

$$\phi_{z_0}(z) \equiv \mathcal{A}f_{z_0}(z) = \frac{\hbar g^2(z)}{\Delta_t}|\langle r|D(z)\rangle|^2 = \frac{\hbar g^2(z)}{\Delta_t}\cos^2\theta(z).$$

We illustrate this focusing function with subwavelength resolution in Fig. 2b for a specific laser configuration.

Microscope Operation – The parameters characterizing the microscope are the spatial resolution $\sigma \ll \lambda$, the temporal resolution τ_c (given essentially by the cavity linewidth $1/\kappa$) and the dispersive atom-cavity coupling controlling the strength of the measurement. To be specific we will illustrate below the operation of the microscope as continuous observation of an atom moving in a harmonic oscillator (HO) potential $V(\hat{z}) = \frac{1}{2}m\omega^2\hat{z}^2$. The corresponding Hamiltonian is $\hat{H}_{\mathrm{sys}} = \hbar\omega(\hat{a}^\dagger\hat{a} + \frac{1}{2})$ with ω the oscillator frequency and $\hat{a}$ ($\hat{a}^\dagger$) lowering (raising) operators for the vibrational eigenstates $|n\rangle$ ($n = 0, 1, \ldots$). The generic physical realization of such a system includes a neutral atom in an optical trap (lattice), or an ion in a Paul trap [4], where we require a spatial resolution better than the length scale set by the HO ground state $\ell_0 = \sqrt{\hbar/m\omega} \gtrsim \sigma$ where m is the atomic mass.

We consider below two modes of operation. In the first, the microscope is placed at a given z_0, and we wish to 'record a movie' of the time dynamics of an atomic wave packet (e.g. a coherent state) passing (repeatedly) through the observation zone. This requires a time resolution better than the oscillation period, and corresponds to the *bad cavity limit* $\kappa \gg \omega$, where according to Eq. (5) the homodyne current as a function
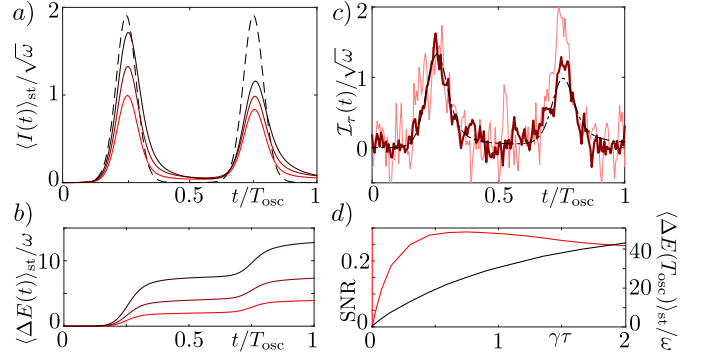

FIG. 3. Monitoring oscillations of a coherent wave packet in a HO ($\alpha = 2$) with a microscope at $z_0 = 0$ and $\sigma = 0.3\ell_0$. a) The ensemble-averaged $\langle I(t)\rangle_{\mathrm{st}}$ over the oscillation period $T_{\mathrm{osc}} = 2\pi/\omega$ with increasing $\gamma/\omega = 1$, 2, and 4 (light to dark). Dashed line indicates the ideal transit signal with no measurement (a. u.). (b) Heating of the atom during measurements. c) Filtered homodyne current for $\gamma = 2\omega$, averaged over 50 (thin) and 300 (thick) scans. d) SNR at the first peak ($t = 0.25T_{\mathrm{osc}}$) for a single scan and the heating for different $\gamma\tau$, with τ the filter integration time (see text).

of time mirrors directly the wave packet motion at z_0 (c.f. Fig. 3, and discussion below). As the second case we consider the *good cavity limit* $\kappa \ll \omega$. Here the observed homodyne signal traces the atomic dynamics at z_0 cavity-averaged over many oscillation periods [30]. However, as we show below, in this regime a *slow scan* of the focal point $z_0 \equiv z_0(t)$ across the spatial region of interest will turn the microscope into an effective QND device, which maps out the spatial density associated with a particular energy eigenfunction of the trapped particle with resolution σ. This will be discussed below in the context of Fig. 1c-e, where a particle is prepared initially in a state $\tilde{\rho}(0) = \sum_n p_n |n\rangle\langle n|$ (e.g. a thermal state), and in the spirit of a QND measurement a *single scan* with the microscope starting at $z_0 = -L/2$ first collapses the atomic state into a particular motional eigenstate, and continuing the scan $-L/2 < z_0 < L/2$ 'takes a picture' of the spatial density of this eigenfunction. This ability of a *single scan* to reveal the density associated with the energy eigenfunction in a QND measurement is in contrast to the first case above, where the measurement is inherently destructive and a good SNR is only obtained with repeated runs of the experiment.

Bad cavity limit and time-resolved dynamics – In Fig. 3a we plot the ensemble averaged homodyne current $\langle I(t)\rangle_{\mathrm{st}}$ for a microscope positioned at $z_0 = 0$, which monitors the periodic motion of an atomic wave packet in the HO. The atom is initially prepared in a coherent state $|\alpha\rangle$ displaced from trap center with $|\alpha| \gg 1$, and the microscope detects the transit of the wave packet with velocity $v = \sqrt{2}\ell_0|\alpha|\omega$ through the trap center at times $t = 1/4$, $3/4T_{\mathrm{osc}}$ etc., with $T_{\mathrm{osc}} = 2\pi/\omega$ the oscillator period. The time dependence of the homodyne current reveals the shape of the wave packet for the given resolution $\sigma =$
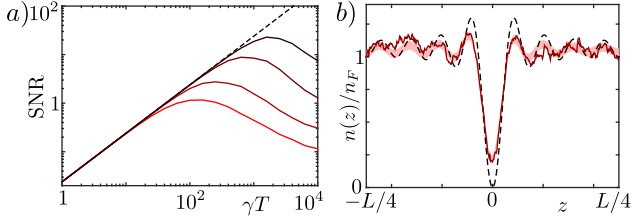
FIG. 4. Single-run scans in the QND regime. a) SNR vs. γT for a scan of an atom initialized in the state $|1\rangle$ of an HO for $\omega/\kappa = 0.1, 1, 4$, and 10 (light to dark), compared to an ideal QND measurement (dashed line) for $\sigma = 0.3\ell_0$ and $L = 8\ell_0$. SNR is taken at $z_0(t) = -\ell_0$ (theoretical maximum). (b) Scan of Friedel oscillations for $N = 16$ non-interacting fermions in a box of length L due to an impurity at $z = 0$: The scanning signal (solid line), the total noise variance (shaded area), and the theoretical density profile $n(z) = n_F[1 - \sin(2k_Fz)/(2k_Fz)]$ (dashed line) with $n_F = k_F/\pi = N/L$.

$0.3\ell_0$. Fig. 3a plots $\langle I(t)\rangle_{\rm st} = 2\sqrt{\gamma}\,{\rm Tr}\,\{f_{z_0}(\hat{z})\tilde{\rho}(t)\}$ for increasing measurement strengths γ, with $\tilde{\rho}(t) \equiv \langle\tilde{\rho}_c(t)\rangle_{\rm st}$ obeying Eq. (5). For the given parameters, Fig. 3a displays the ability of the homodyne current to faithfully represent the temporal shape of the wave packet, and reveals the measurement backaction with increasing γ as a successive distortion of the signal with time. Fig. 3b quantifies this backaction as an increase of the mean energy of the oscillator with time.

The SNR associated with these measurements is shown in Figs. 3c-d. We define the SNR as $\langle\mathcal{I}_\tau(t)\rangle_{\rm st}^2/\langle\delta\mathcal{I}_\tau^2(t)\rangle_{\rm st}$ with $\mathcal{I}_\tau(t) \equiv \int_\tau I(t+t')dt'/\sqrt{\tau}$ the homodyne current (2) after a lowpass filter with bandwidth τ^{-1}, and the variance $\langle\delta\mathcal{I}_\tau^2(t)\rangle_{\rm st} \equiv \langle\mathcal{I}_\tau^2(t)\rangle_{\rm st} - \langle\mathcal{I}_\tau(t)\rangle_{\rm st}^2$. We choose an integration time τ sufficiently long to suppress the shot noise, but short enough to resolve the temporal shape of the wave packet propagation. An optimal τ is related to the spatial resolution of the microscope, $\tau \sim \sigma/v = (\sigma/\ell_0)\tau_{\rm tr}$ with $\tau_{\rm tr}$ the transit time of the wave packet through the focal region. In Fig. 3c we show a simulation of the homodyne current $\mathcal{I}_\tau(t)$ averaged over an increasing number of measurements, and the convergence to the results of Fig. 3a. In Fig. 3d the SNR in a single scan is plotted vs. the measurement strength γ. It shows the general behavior of non-QND measurements [31]: For small γ, the SNR grows with increasing γ due to suppression of the shot noise. For large γ, SNR eventually drops down as the measurement backaction induces strong additional noises.

Good cavity limit as emergent QND measurement – A QND measurement requires that the associated observable commutes with the system Hamiltonian. While $f_{z_0}(\hat{z})$ does not commute with $\hat{H}_{\rm sys}$, an effective QND measurement emerges in the good cavity limit $\kappa \ll \omega$. We can see this by transforming the SME (3) to an interaction picture with respect to $\hat{H}_{\rm sys}$. This transformation results in the replacement $f_{z_0}(\hat{z}) \to \sum_\ell \hat{f}_{z_0}^{(\ell)} e^{-i\ell\omega t}$, where $\hat{f}_{z_0}^{(\ell)} = \sum_n f_{n,n+\ell}|n\rangle\langle n+\ell|$ with $f_{mn} = \langle m|f_{z_0}(\hat{z})|n\rangle$. In a

homodyne measurement, where the current $I(t)$ is monitored with time resolution $1/\kappa$, as filtered by a good cavity, the terms rapidly oscillating with the trap frequency (motional sidebands) will not be resolved. Thus homodyne detection provides a continuous measurement of $\hat{f}_{z_0}^{(0)} = \sum_n f_{n,n}|n\rangle\langle n|$ representing the emergent QND observable.

A formal derivation of these results is provided in Appendix B starting from the SME (3). There we derive for the homodyne current $dX_\phi(t) \equiv I(t)dt = 2\sqrt{\gamma}\,\langle\hat{f}_{z_0}^{(0)}\rangle_c + dW(t)$ with $\langle\ldots\rangle_c = {\rm Tr}\{\ldots\tilde{\rho}_c(t)\}$, where the conditional density operator $\tilde{\rho}_c(t)$ obeys the SME

$$d\tilde{\rho}_c = -\frac{i}{\hbar}[\hat{H}_{\rm sys}, \tilde{\rho}_c]\,dt + \sum_{\ell\neq0}\frac{\gamma}{1+(2\omega\ell/\kappa)^2}\mathcal{D}[\hat{f}_{z_0}^{(\ell)}]\tilde{\rho}_c\,dt$$
$$+ \gamma\mathcal{D}[\hat{f}_{z_0}^{(0)}]\tilde{\rho}_c\,dt + \sqrt{\gamma}\mathcal{H}[\hat{f}_{z_0}^{(0)}]\tilde{\rho}_c\,dW(t), \qquad (6)$$

with γ the measurement strength defined above (assuming resonant driving). To provide a physical interpretation, we take matrix elements of Eq. (6) in the energy eigenbases and obtain a (nonlinear) *stochastic rate equation* (SRE) for the trap-state populations $p_n = \langle n|\tilde{\rho}_c|n\rangle$:

$$dp_n = \frac{\gamma}{1+(2\omega/\kappa)^2}\left[A_n^{(+)}p_{n+1} + A_n^{(-)}p_{n-1} - B_np_n\right]dt$$
$$+ 2\sqrt{\gamma}p_n\left[f_{nn} - \sum_m f_{mm}p_m\right]dW(t). \qquad (7)$$

Here $A_n^{(\pm)} \equiv |f_{n,n\pm1}|^2$, $B_n \equiv A_n^{(+)} + A_n^{(-)}$, and for simplicity we have kept only the dominant terms $\ell = 0, \pm1$ for $\kappa/\omega \ll 1$. We emphasize that Eq. (7) involves two time scales. The stochastic term in the second line describes the collapse of the density operator to a particular trap eigenstate $\tilde{\rho}_c(t) \to |n\rangle\langle n|$ within a collapse time $T_{\rm coll} \sim 1/\gamma$. In contrast, the first line is a redistribution of population between the trap levels, for a much longer dwell time $T_{\rm dwell} \sim (2\omega/\kappa)^2\gamma^{-1} \gg T_{\rm coll}$. As a result, the time evolution consists of a rapid collapse to an energy eigenstate $|n\rangle$, followed by a sequence of rare quantum jumps $n \to n\pm1$ on the time scale $T_{\rm dwell}$. The QND mode of the microscope exploits these two time scales by scanning the focal point across the system, $-L/2 < z_0(t) < L/2$, in a time $T_{\rm coll} \ll T \lesssim T_{\rm dwell}$. Starting the measurement scan, the motional state will first collapse to a particular state $|n\rangle$, with the subsequent scan revealing the spatial density profile $\langle n|\hat{f}_{z_0}^{(0)}|n\rangle = \int dz\, f_{z_0}(z)|\langle z|n\rangle|^2$.

Fig. 1c shows a simulation representing a *single run* in the QND regime ($\kappa/\omega = 0.1$) based on integrating the SME (6). The atom at $t = 0$ is prepared in a thermal motional state of the HO, $\tilde{\rho}(0) = \sum_n p_n|n\rangle\langle n|$ with $n_{\rm th} = 0.6$. We perform three consecutive spatial scans covering $-L/2 < z_0(t) < L/2$ ($L = 10\ell_0$), each in a time interval T ($\gamma T = 5000$). For the run shown in Figs. 1c-e, the QND measurement in *scan 1* first projects the atomic trap population into $|0\rangle$, followed by a transition to $|1\rangle$ at time t_1, and $|1\rangle \to |0\rangle$ at t_2 in *scan 2*, and no transition in *scan 3*. The homodyne current $\mathcal{I}_\tau(t)$ associated with these single scans is a faithful representation of the

spatial density distributions of eigenfunctions $|\langle z|n\rangle|^2$. In Fig. 4a the SNR of single scans of a pure state is shown against the (dimensionless) measurement strength γT. By increasing ω/κ we greatly suppress the measurement back-action, rendering them into rarer quantum jumps, thus improving the SNR.

The concept of a scanning microscope to observe *in vivo* cold atom dynamics is readily adapted to a quantum many-body system, and we show in Fig. 4b a spatial scan of the Friedel oscillation of an non-interacting Fermi sea in the presence of a single impurity (with details found in Appendix C). While we have focused on homodyne measurement in CQED for continuous readout, atomic

physics setups provide interesting alternative routes to achieve weak continuous measurement, e.g. coupling to atomic ensembles via Rydberg interactions [32–34].

[1] For a review, see S. Kuhr, National Science Review **3**, 170 (2016) and references therein.
[2] V. B. Braginsky and F. Y. Khalili, *Quantum Measurement* (CUP, Cambridge, 1992).
[3] H. M. Wiseman and G. J. Milburn, *Quantum measurement and control* (CUP, Cambridge, 2009).
[4] C. Gardiner and P. Zoller, *The Quantum World of Ultra-Cold Atoms and Light Book II* (ICP, London, 2015).
[5] For recent reviews, see I. B. Mekhov and H. Ritsch, Journal of Physics B: Atomic, Molecular and Optical Physics **45**, 102001 (2012); H. Ritsch, P. Domokos, F. Brennecke, and T. Esslinger, Rev. Mod. Phys. **85**, 553 (2013); T. E. Northup and R. Blatt, Nat. Photon. **8**, 356 (2014); A. Reiserer and G. Rempe, Rev. Mod. Phys. **87**, 1379 (2015).
[6] Continuous observation of classical atomic motion in Cavity QED is demonstrated in C. J. Hood, T. W. Lynn, A. C. Doherty, A. S. Parkins, and H. J. Kimble, Science **287**, 1447 (2000); T. Puppe, I. Schuster, A. Grothe, A. Kubanek, K. Murr, P. W. H. Pinkse, and G. Rempe, Phys. Rev. Lett. **99**, 013002 (2007); M. L. Terraciano, R. Olson Knell, D. G. Norris, J. Jing, A. Fernandez, and L. A. Orozco, Nat. Phys. **5**, 480 (2009).
[7] Strong measurement of quantum particles with sub-wavelength resolution is demonstrated, e.g., in P. C. Maurer, J. R. Maze, P. L. Stanwix, L. Jiang, A. V. Gorshkov, A. A. Zibrov, B. Harke, J. S. Hodges, A. S. Zibrov, A. Yacoby, D. Twitchen, S. W. Hell, R. L. Walsworth, and M. D. Lukin, Nat. Phys. **6**, 912 (2010); F. Zähringer, G. Kirchmair, R. Gerritsma, E. Solano, R. Blatt, and C. F. Roos, Phys. Rev. Lett. **104**, 100503 (2010).
[8] For QND measurements in quantum optics, see, e.g., S. Gleyzes, S. Kuhr, C. Guerlin, J. Bernu, S. Deleglise, U. Busk Hoff, M. Brune, J.-M. Raimond, and S. Haroche, Nature **446**, 297 (2007); B. R. Johnson, M. D. Reed, A. A. Houck, D. I. Schuster, L. S. Bishop, E. Ginossar, J. M. Gambetta, L. DiCarlo, L. Frunzio, S. M. Girvin, and R. J. Schoelkopf, Nat. Phys. **6**, 663 (2010); C. B. Møller, R. A. Thomas, G. Vasilakis, E. Zeuthen, Y. Tsaturyan, M. Balabas, K. Jensen, A. Schliesser, K. Hammerer, and E. S. Polzik, Nature **547**, 191 (2017).
[9] K. D. Stokes, C. Schnurr, J. R. Gardner, M. Marable, G. R. Welch, and J. E. Thomas, Phys. Rev. Lett. **67**, 1997 (1991).
[10] C. Weitenberg, M. Endres, J. F. Sherson, M. Cheneau,

P. Schausz, T. Fukuhara, I. Bloch, and S. Kuhr, Nature **471**, 319 (2011).
[11] A. V. Gorshkov, L. Jiang, M. Greiner, P. Zoller, and M. D. Lukin, Phys. Rev. Lett. **100**, 093005 (2008).
[12] A. Stute, B. Casabone, P. Schindler, T. Monz, P. O. Schmidt, B. Brandstatter, T. E. Northup, and R. Blatt, Nature **485**, 482 (2012).
[13] M. Wolke, J. Klinner, H. Keßler, and A. Hemmerich, Science **337**, 75 (2012).
[14] B. Hacker, S. Welte, G. Rempe, and S. Ritter, Nature **536**, 193 (2016).
[15] J. Léonard, A. Morales, P. Zupancic, T. Esslinger, and T. Donner, Nature **543**, 87 (2017).
[16] A. J. Kollár, A. T. Papageorge, V. D. Vaidya, Y. Guo, J. Keeling, and B. L. Lev, Nat. Commun. **8**, 14386 (2017).
[17] J. D. Thompson, T. G. Tiecke, N. P. de Leon, J. Feist, A. V. Akimov, M. Gullans, A. S. Zibrov, V. Vuletić, and M. D. Lukin, Science **340**, 1202 (2013).
[18] C. Junge, D. O'Shea, J. Volz, and A. Rauschenbeutel, Phys. Rev. Lett. **110**, 213604 (2013).
[19] A. Goban, C.-L. Hung, S.-P. Yu, J. D. Hood, J. A. Muniz, J. H. Lee, M. J. Martin, A. C. McClung, K. S. Choi, D. E. Chang, O. Painter, and H. J. Kimble, Nat. Commun. **5**, 3808 (2014).
[20] H. L. Sørensen, J.-B. Béguin, K. W. Kluge, I. Iakoupov, A. S. Sørensen, J. H. Müller, E. S. Polzik, and J. Appel, Phys. Rev. Lett. **117**, 133604 (2016).
[21] D. A. Steck, K. Jacobs, H. Mabuchi, T. Bhattacharya, and S. Habib, Phys. Rev. Lett. **92**, 223004 (2004).
[22] A. C. J. Wade, J. F. Sherson, and K. Mølmer, Phys. Rev. Lett. **115**, 060401 (2015).
[23] G. Mazzucchi, S. F. Caballero-Benitez, D. A. Ivanov, and I. B. Mekhov, Optica **3**, 1213 (2016).
[24] Y. Ashida and M. Ueda, Phys. Rev. A **95**, 022124 (2017).
[25] C. Laflamme, D. Yang, and P. Zoller, Phys. Rev. A **95**, 043843 (2017).
[26] H. Carmichael, *An Open Systems Approach to Quantum Optics* (Springer, Berlin, 1993).
[27] We contrast this to schemes where $I(t)$ reflects the atomic positon $\langle \hat{z}\rangle_c$ in, e.g. R. Quadt, M. Collett, and D. F. Walls, Phys. Rev. Lett. **74**, 351 (1995); T. Konrad, A. Rothe, F. Petruccione, and L. Diósi, New J. Phys. **12**, 043038 (2010).
[28] M. Łacki, M. A. Baranov, H. Pichler, and P. Zoller, Phys.

Rev. Lett. **117**, 233001 (2016).

[29] F. Jendrzejewski, S. Eckel, T. G. Tiecke, G. Juzeliūnas, G. K. Campbell, L. Jiang, and A. V. Gorshkov, Phys. Rev. A **94**, 063422 (2016).

[30] This situation is reminiscent of the sideband resolved laser cooling of trapped particles in the Lamb-Dicke limit where $\gamma \ll \omega$ with γ optical pumping rate [4].

[31] A. A. Clerk, M. H. Devoret, S. M. Girvin, F. Marquardt, and R. J. Schoelkopf, Rev. Mod. Phys. **82**, 1155 (2010).

[32] M. Saffman, T. G. Walker, and K. Mølmer, Rev. Mod. Phys. **82**, 2313 (2010).

[33] H. Labuhn, D. Barredo, S. Ravets, S. de Léséleuc, T. Macrì, T. Lahaye, and A. Browaeys, Nature **534**, 667 (2016).

[34] H. Bernien, S. Schwartz, A. Keesling, H. Levine, A. Omran, H. Pichler, S. Choi, A. S. Zibrov, M. Endres, M. Greiner, V. Vuletić, and M. D. Lukin, arXiv:1707.04344.

[35] O. Černotík, D. V. Vasilyev, and K. Hammerer, Phys. Rev. A **92**, 012124 (2015).

Appendix A: Engineering of The Sub-wavelength Focusing Function $\phi_{z_0}(z)$

Here we discuss in detail the realization of the focusing function $\phi_{z_0}(z)$ [c.f. Eq. (1) of the main text], showing that subwavelength resolution can be achieved along with negligible additional forces on the atom.

1. Sub-wavelength spin structure with negligible non-adiabatic potential

The atomic internal levels for implementing the focusing function, shown in Fig. 2 of the main text, consists of a Λ-system formed by $|g\rangle, |r\rangle, |e\rangle$, described by the Hamiltonian

$$\hat{H}_\mathrm{a} = -\hbar \left(\Delta_e + i \frac{\Gamma_e}{2} \right) \hat{\sigma}_{ee} + \frac{\hbar}{2} \left[\Omega_0(z)\hat{\sigma}_{eg} + \Omega_1(z)\hat{\sigma}_{er} + \mathrm{H.c.} \right],$$
(A1)

where Γ_e is the decay rate of the excited state, and we assume Raman resonance $\Delta_r = 0$. Diagonalizing $\hat{H}_\mathrm{a}$ gives the eigenstates

$$|D(z)\rangle = \sin\theta(z) |g\rangle - \cos\theta(z) |r\rangle ,$$
$$|+(z)\rangle = \cos\chi(z) |e\rangle + \sin\chi(z)[\cos\theta(z) |g\rangle + \sin\theta(z) |r\rangle],$$
$$|-(z)\rangle = \sin\chi(z) |e\rangle - \cos\chi(z)[\cos\theta(z) |g\rangle + \sin\theta(z) |r\rangle],$$
(A2)

with the corresponding eigenenergies $E_D = 0$ and $E_\pm(z) = -(\hbar/2)\{\tilde{\Delta}_e \mp [\Omega_0^2(z) + \Omega_1^2(z) + \tilde{\Delta}_e^2]^{1/2}\}$, where $\tilde{\Delta}_e = \Delta_e + i\Gamma_e/2$, and the mixing angles defined by $\theta(z) = \arctan[\Omega_1(z)/\Omega_0(z)]$ and $\chi(z) = -(1/2)\arctan[\sqrt{\Omega_0^2(z) + \Omega_1^2(z)}/\tilde{\Delta}_e]$. We note that the *dark state* $|D(z)\rangle$ is decoupled from the dissipative excited state $|e\rangle$, and its spin structure is varying in space controlled by the Rabi frequency configuration.

We are interested in the regime where $\mathrm{Re}[E_\pm(z)]$ is much larger than the other energy scales in the model. In the spirit of the Born-Oppenheimer (BO) approximation, we study the *slow dynamics* by assuming the atomic internal state remains in $|D(z)\rangle$ adiabatically. This allows us to design the desired sub-wavelength spin structure $|\langle r|D(z)\rangle|^2 = \cos^2\theta$. Such a spatially varying internal spin is, however, necessarily accompanied by non-adiabatic corrections to the atomic external motion [28, 29]

$$V_{na}(z) = \langle D(z)| \frac{\hat{p}_z^2}{2m} |D(z)\rangle = \frac{\hbar^2}{2m}[\partial_z \theta(z)]^2. \quad (A3)$$

We now show that $|\langle r|D(z)\rangle|^2$ can be made nano-scale with negligible $V_{na}(z)$. We consider the Rabi frequencies

$$\Omega_0(z) = \epsilon\Omega_c,$$
$$\Omega_1(z) = \Omega_c[1 + \beta + \sin k_1(z - z_0)],$$
(A4)

where Ω_c is a large reference frequency (assumed real positive) and $0 < \epsilon \sim \beta \ll 1$. Physically, $\Omega_1(z)$ can

be realized, e.g., by super-imposing three phase-coherent laser beams where the first two lasers form the standing wave $\Omega_c \sin k_1(z - z_0)$, and the third propagates perpendicularly, to provide the offset $\Omega_c(1 + \beta)$.

For Rabi frequencies in Eq. (A4), the resolution σ, quantified by the full width at half maximum (FWHM) of $|\langle r|D(z)\rangle|^2$, is given in the limit $\epsilon \ll 1$ by

$$\sigma = \frac{\sqrt{2}\lambda_1}{\pi} \left(\sqrt{\epsilon^2 + 2\beta^2} - \beta \right)^{1/2}, \qquad \text{(A5)}$$

with $\lambda_1 = 2\pi/k_1$. The non-adiabatic potential is

$$V_{na}(z) = \frac{\hbar^2 k_1^2}{2m\epsilon^2} \left(\frac{\cos k_1(z - z_0)}{1 + [1 + \beta + \sin k_1(z - z_0)]^2/\epsilon^2} \right)^2. \qquad \text{(A6)}$$

Importantly, $V_{na}(z)$ decreases rapidly by increasing the ratio β/ϵ, as shown in Fig. 5. Physically, increasing β/ϵ reduces the maximal population transfer onto the state $|r\rangle$ during the adiabatic motion, $|\langle r|D(z)\rangle|^2_{\max} = (1 + \beta^2/\epsilon^2)^{-1}$, thus suppressing the corresponding non-adiabatic potential. This sub-wavelength spin structure, with negligible $V_{na}(z)$, is exploited to realize the focusing function $\phi_{z_0}(z)$, as we show below.

2. Sub-wavelength focusing function $\phi_{z_0}(z)$

In addition to the Λ-system, we couple the level $|r\rangle$ to $|t\rangle$ dispersively through a cavity mode $\hat{c}$, described by the Hamiltonian $\hat{H}_{ac} = \hbar g(\hat{z})^2 \hat{c}^\dagger \hat{c}/\Delta_t$. Projecting it into the dark state $|D(z)\rangle$ in the BO approach leads to the desired sub-wavelength atom-cavity coupling

$$\hat{H}_{coup} = \frac{\hbar g^2(z)}{\Delta_t} |\langle r|D(z)\rangle|^2 \hat{c}^\dagger \hat{c} \equiv \phi_{z_0}(z) \hat{c}^\dagger \hat{c}, \qquad \text{(A7)}$$

with its resolution given by Eq. (A5) [notice $g(z)$ varies slowly compared to σ].

Through this sub-wavelength coupling, the stationary coherent field inside the driven cavity will exert forces on the atom, $V_{OL}(z) = \hbar g^2(z)|\alpha|^2|\langle r|D(z)\rangle|^2/\Delta_t$, with $\alpha = \sqrt{\kappa}\mathcal{E}(i\delta - \kappa/2)^{-1}$ being the amplitude of the stationary field, (δ and $\mathcal{E}$ is the detuning and strength of the cavity driving laser respectively). Such a force can be compensated by simply detuning the Raman resonance with an appropriate offset $\Delta_r = g^2(z_0)|\alpha|^2/\Delta_t$ (c.f. Fig. 2a in the main text), which, after projection onto $|D(z)\rangle$, picks up an additional factor $|\langle r|D(z)\rangle|^2$ and, thanks to the subwavelength width of this factor, compensates $V_{OL}(z)$ nearly perfectly.

In the above BO analysis we assume $|D(z)\rangle$ to have an infinite lifetime. Couplings between $|D(z)\rangle$ and $|\pm(z)\rangle$, from either the atomic kinetic term or $\hat{H}_{coup}$ (and the compensation offset Δ_r), will cause spontaneous decay of the dark state thus limiting its lifetime. Nevertheless, the decay rate γ_D of $|D(z)\rangle$ is greatly suppressed by large Rabi frequencies, with a general scaling $\gamma_D \propto [\Omega_1^2(z) + \Omega_0^2(z)]^{-2}$ [28]. By choosing large enough Rabi
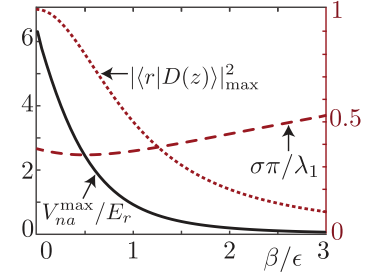

FIG. 5. The resolution σ and the maximum of the non-adiabatic potential $V_{na}(z)$ [c.f., Eq. (A3), in unit of the recoil energy $E_r = \hbar^2 k_1^2/2m$], vs. β/ϵ, for the laser configuration Eq. (A4). Also shown is the maximum overlap between $|D(z)\rangle$ and $|r\rangle$. Parameters: $\epsilon = 0.1$. We note that $V_{na}(z)$ is strongly suppressed for $\beta/\epsilon \gg 1$.

frequencies, we can neglect this unwanted dissipation within the relevant timescale of experiments.

The focusing function $\phi_{z_0}(z)$ realized by Eq. (A4) has multiple peaks separated by λ_1. To design a single-peak $\phi_{z_0}(z)$ one can simply choose $\Omega_0(z)$ being tightly focused at z_0 to suppress the other peaks.

As mentioned in the main text, it is convenient to write $\phi_{z_0}(z) \equiv \mathcal{A}f_{z_0}(z)$ with $f_{z_0}(z)$ dimensionless and normalized, and $\mathcal{A}$ a constant with the dimensions of energy. We choose the normalization $\int dz f_{z_0}(z) = \ell_0$ with ℓ_0 the characteristic length scale of the system under measurement, such that the matrix elements of $f_{z_0}(\hat{z})$ are of order 1.

Appendix B: Perturbative Elimination of the Cavity Field

In this section we consider the relation between the homodyne current $I(t)$ and the localised microscope probe $f_{z_0}(\hat{z})$. To obtain the connection we eliminate the cavity field from the stochastic dynamics described by the Eq. (3) in the main text. The aim is to derive effective stochastic master equations (5) and (6) with corresponding photocurrents in 'bad' and 'good' cavity limits respectively.

To make the discussion more general, first, we consider an arbitrary system which is coupled to the cavity field $\hat{c}$ via interaction $\hat{H}_{int} = \hbar\varepsilon\hat{f}(\hat{c} + \hat{c}^\dagger)$ where $\hat{f}$ is a system operator and the coupling is assumed to be weak compared to the cavity decay rate $\varepsilon \ll \kappa$. This model is related to the atomic system from the main text coupled to a driven cavity via the interaction (1) linearised around the steady state intracavity field.

Transforming to an interaction picture with respect to the system Hamiltonian $\hat{H}_{sys}$ we obtain the following SME describing the dynamics of the full setup under continuous homodyne monitoring of the cavity output

field:

$$dρ_c = -i[ε\hat{f}(t)(\hat{c} + \hat{c}^†) + δ\hat{c}^†\hat{c}, ρ_c]dt + κ\mathcal{D}[\hat{c}]ρ_c dt$$
$$+ \sqrt{κ}\mathcal{H}[\hat{c}e^{-iφ}]ρ_c dW(t), \tag{B1}$$

where $δ$ is the cavity detuning, $φ$ is the homodyne angle, and $\hat{f}(t) = e^{i\hat{H}_{\text{sys}}t}\hat{f}e^{-i\hat{H}_{\text{sys}}t}$. The corresponding homodyne current reads:

$$dX_φ(t) \equiv I(t)dt = \sqrt{κ}\left\langle \hat{c}e^{-iφ} + \hat{c}^†e^{iφ}\right\rangle_c dt + dW(t) \tag{B2}$$

where $\langle\dots\rangle_c \equiv \text{Tr}\{\dots ρ_c(t)\}$ refers to an expectation value with respect to the conditional density matrix. We eliminate the cavity field along the lines of [35]. First, we simply trace out the cavity dynamics from the SME (B1) to obtain a stochastic equation for the system density matrix only ($\tilde{ρ}_c = \text{Tr}_T ρ_c$):

$$d\tilde{ρ}_c = -iε\left[\hat{f}(t), \hat{η} + \hat{η}^†\right]dt + \sqrt{κ}\left(\hat{μ}e^{-iφ} + \hat{μ}^†e^{iφ}\right)dW(t) \tag{B3}$$

where we define operators $\hat{η} = \text{Tr}_T\{\hat{c}ρ_c\}$ and $\hat{μ} = \hat{η} - \langle\hat{c}\rangle\tilde{ρ}_c$ such that $\langle\hat{c}\rangle = \text{Tr}_S\hat{η}$, and operations Tr_T and Tr_S stand for the partial traces over states of the cavity (T for transducer) and the system respectively. We derive an effective equation for $\tilde{ρ}_c$ up to the second order in the perturbation $ε$ for the deterministic term and up to a linear stochastic term: $d\tilde{ρ}_c = O(ε^2)dt + O(ε)dW(t)$. This restricts equations for the operators $\hat{η}$ and $\hat{μ}$ to $d\hat{η}(d\hat{μ}) = O(ε)dt + O(1)dW(t)$. The equation of motion for $η$ operator reads

$$d\hat{η} = \text{Tr}_T\{\hat{c}\,dρ\}$$
$$= -iε\text{Tr}_T\left\{\hat{c}\left[\hat{f}(t)(\hat{c} + \hat{c}^†), ρ\right]\right\}dt - \left(\frac{κ}{2} - iδ\right)\hat{η}\,dt$$
$$+ \sqrt{κ}\,\text{Tr}_T\left\{\hat{c}(\hat{c}ρ - \langle\hat{c}\rangle ρ)e^{-iφ} + \hat{c}(ρ\hat{c}^† - \langle\hat{c}^†\rangle ρ)e^{iφ}\right\}dW(t)$$
$$\simeq -iε\hat{f}(t)\tilde{ρ}_c dt - \left(\frac{κ}{2} - iδ\right)\hat{η}\,dt \tag{B4}$$

in the first deterministic term and in the stochastic term we used the fact that $ρ = \tilde{ρ}_c \otimes ρ_T$ to zeroth order in $ε$ and that the unperturbed cavity is in a vacuum steady state such that $\langle\hat{c}\hat{c}^†\rangle = 1$, $\langle\hat{c}\hat{c}\rangle = \langle\hat{c}^†\hat{c}\rangle = 0$. Next, for the cavity mean field we have:

$$d\langle\hat{c}\rangle = \text{Tr}_S d\hat{η}$$
$$\simeq -iε\langle\hat{f}(t)\rangle dt - \left(\frac{κ}{2} - iδ\right)\langle\hat{c}\rangle dt \tag{B5}$$

This equation is first order in $ε$ which means, to define operator $\hat{μ}$, we need to know $\tilde{ρ}_c$ to the zeroth order in $ε$. It is constant in this approximation ($d\tilde{ρ}_c = 0$) and we obtain an equation for the $\hat{μ}$ operator using Itô rule:

$$d\hat{μ} = d\hat{η} - \{(d\langle\hat{c}\rangle)\tilde{ρ}_c + \langle\hat{c}\rangle d\tilde{ρ}_c + (d\langle\hat{c}\rangle)d\tilde{ρ}_c\}$$
$$\simeq -iε\left\{\hat{f}(t) - \langle\hat{f}(t)\rangle\right\}\tilde{ρ}_c dt - \left(\frac{κ}{2} - iδ\right)\hat{μ}\,dt \tag{B6}$$

Plugging the solutions of the Eqs. (B4) and (B6) into the equation of motion for the system density operator (B3)

we recover an effective equation with the necessary precision in $ε$. There are two cases to consider.

'Bad' cavity — If the free evolution of the system can be neglected on a time scale of the cavity decay $1/κ$ (for our harmonic oscillator $κ \gg ω$) we obtain:

$$\hat{η} \simeq -iε\frac{\hat{f}(t)}{κ/2 - iδ}\tilde{ρ}_c, \qquad \hat{μ} \simeq -iε\frac{\hat{f}(t) - \langle\hat{f}(t)\rangle}{κ/2 - iδ}\tilde{ρ}_c.$$

Substituting these expressions into the Eq. (B3) and restoring the Schrödinger picture we arrive at the effective SME:

$$d\tilde{ρ}_c = -\frac{i}{\hbar}[\hat{H}_{\text{eff}}, \tilde{ρ}_c]dt + γ\mathcal{D}[\hat{f}]\tilde{ρ}_c dt + \sqrt{γ}\mathcal{H}[\hat{f}]\tilde{ρ}_c dW(t) \tag{B7}$$

where $\hat{H}_{\text{eff}} = \hat{H}_{\text{sys}} + (\hbar\,δ\,ε^2\hat{f}^2)/\{(κ/2)^2 + δ^2\}$ and $γ = (ε^2κ)/\{(κ/2)^2 + δ^2\}$. The homodyne phase is chosen to maximize the signal in the photocurrent ($φ = -π/2 + \arctan\{2δ/κ\}$) such that

$$dX_φ(t) \equiv I(t)dt = 2\sqrt{γ}\langle\hat{f}\rangle_c dt + dW(t) \tag{B8}$$

which is obtained by substituting solution of Eq. (B5) into Eq. (B2). In the main text we consider the cavity driven by a coherent field $\mathcal{E}$ such that the coupling coefficient is given by $ε = (\mathcal{A}\mathcal{E}/\hbar)\{κ/(κ^2/4+δ^2)\}^{1/2}$. Defining $\hat{f} = f_{z_0}(\hat{z})$ and setting zero detuning $δ = 0$ the equations (B8) and (B7) become Eqs. (4) and (5) in the main text.

Ensemble averaging the stochastic dynamics (B7) over individual trajectories results in the corresponding ME for the unconditional density matrix $\tilde{ρ}(t) = \langle\tilde{ρ}_c(t)\rangle_{\text{st}}$:

$$\frac{d\tilde{ρ}}{dt} = -\frac{i}{\hbar}[\hat{H}_{\text{eff}}, \tilde{ρ}] + γ\mathcal{D}[\hat{f}]\tilde{ρ}.$$

Here we used the non-anticipating property of the stochastic differential equation in Itô form $\langle\dots dW(t)\rangle_{\text{st}} = 0$.

'Good' cavity — In the case of harmonic oscillator $\hat{H}_{\text{sys}} = \hbar ω(\hat{a}^†\hat{a} + 1/2)$ the system coupling operator (localised probe $f_{z_0}(\hat{z})$) in the interaction picture reads $\hat{f}(t) = \sum_\ell \hat{f}^{(\ell)}e^{-i\ell ω t}$, where $\hat{f}^{(\ell)} = \sum_n f_{n,n+l}|n\rangle\langle n + \ell|$ with $f_{mn} = \langle m|f_{z_0}(\hat{z})|n\rangle$. This allows one to integrate Eq. (B4) and (B6) assuming slow time dependence of $\tilde{ρ}_c$ as follows:

$$\hat{η} \simeq -iε\sum_\ell \frac{\hat{f}^{(\ell)}e^{-i\ell ω t}}{κ/2 - i(δ + ω\ell)}\tilde{ρ}_c$$

$$\hat{μ} \simeq -iε\sum_\ell \frac{\left\{\hat{f}^{(\ell)} - \langle\hat{f}^{(\ell)}\rangle\right\}e^{-i\ell ω t}}{κ/2 - i(δ + ω\ell)}\tilde{ρ}_c$$

Substituting the results into the Eq. (B3), keeping only non-rotating deterministic terms due to $κ \ll ω$ in the 'good' cavity limit (secular approximation), and trans-

forming back to the Schrödinger picture we obtain:

$$d\tilde{\rho}_c = -\frac{i}{\hbar}[\hat{H}_{\text{eff}}, \tilde{\rho}_c]dt + \sum_\ell \frac{\varepsilon^2 \kappa}{(\kappa/2)^2 + (\delta + \omega\ell)^2} \mathcal{D}\left[\hat{f}^{(\ell)}\right]\tilde{\rho}_c dt$$
$$+ \varepsilon\sqrt{\kappa}\sum_\ell \mathcal{H}\left[\frac{-ie^{-i\phi}}{\kappa/2 - i(\delta + \omega\ell)}\hat{f}^{(\ell)}\right]\tilde{\rho}_c dW(t), \quad \text{(B9)}$$

where

$$\hat{H}_{\text{eff}} = \hat{H}_{\text{sys}} + \sum_\ell \frac{\hbar\varepsilon^2(\delta + \omega\ell)}{(\kappa/2)^2 + (\delta + \omega\ell)^2}\left(\hat{f}^{(\ell)}\hat{f}^{(\ell)\dagger} - \hat{f}^{(\ell)\dagger}\hat{f}^{(\ell)}\right).$$

To enhance the signal from the QND observable $\hat{f}^{(0)}$ we choose the cavity detuning $\delta = 0$ and the homodyne angle $\phi = -\pi/2$. Then, by filtering out sidebands with $\ell \neq 0$ from the signal, we obtain a homodyne current (again using Eqs. (B2) and (B5)):

$$dX_\phi(t) \equiv I(t)dt = 2\sqrt{\gamma}\langle\hat{f}^{(0)}\rangle_c dt + dW(t) \quad \text{(B10)}$$

with $\gamma = 4\varepsilon^2/\kappa$ and ε defined above. This gives expression for the photocurrent preceding Eq. (6) in the main text. Discarding the sidebands from the photocurrent leads to averaging the effective SME (B9) over corresponding unobserved measurements. This results in dropping stochastic terms with $\ell \neq 0$ from the equation and yields the SME (6) in the paper. In the 'good' cavity limit $\kappa \ll \omega$, the additional part in the Hamiltonian $\hat{H}_{\text{eff}}$ is much smaller than $\hat{H}_{\text{sys}}$ and can be neglected.

Appendix C: Scanning Many-body Systems and the Friedel Oscillation

Here we extend the scanning measurement to the many-body case and provide the details on scanning Friedel oscillations discussed in the main text.

To derivation the SME describing the scan of a many-body system, we decompose the focusing function, $\phi_{z_0}(z) = \mathcal{A}f_{z_0}(z)$ [c.f., Eq. (1) of the main text], in terms of *many-body* eigenstates,

$$\sum_{i=1}^N f_{z_0}(\hat{z}_i) \rightarrow \hat{f}_{z_0} = \sum_{\vec{\nu},\vec{\nu}'} f_{\vec{\nu}\vec{\nu}'}|\vec{\nu}\rangle\langle\vec{\nu}'|, \quad \text{(C1)}$$

where $\vec{\nu}$ is the set of quantum numbers specifying the many-body state $|\vec{\nu}\rangle$ with eigenenergy $E_{\vec{\nu}}$, and $f_{\vec{\nu}\vec{\nu}'} = \langle\vec{\nu}|\sum_i f_{z_0}(\hat{z}_i)|\vec{\nu}'\rangle$ are the matrix elements (Note, being a single-particle operator, $\hat{f}_{z_0}$ generates only single-particle transitions). Let us now define a set $\{\Delta E_j\}$ of difference between the eigenenergies, $\Delta E_j = E_{\vec{\nu}} - E_{\vec{\nu}'}$, for all pairs of eigenstates appearing in Eq. (C1), and define the associated operators

$$\hat{f}^{(\Delta E_j)} = f_{\vec{\nu}\vec{\nu}'}|\vec{\nu}\rangle\langle\vec{\nu}'|,$$

so that $\hat{f}_{z_0} = \sum_j \hat{f}^{(\Delta E_j)}$. Note that here we assume all ΔE_j being different [except for $\Delta E_j = 0$ corresponding to diagonal contributions of (C1)], as in the example of fermions in a box considered below. In situations where there are (quasi-)degenerate energy differences ΔE_j, like atoms in a harmonic trap, the definition of the operators $\hat{f}^{(\Delta E_j)}$ should include the summation over the pairs of states with (quasi) degenerate ΔE_j. The operators $\hat{f}^{(\Delta E_j)}$ are generalizations of $\hat{f}^{(\ell)}$ in the single-particle case in Appendix B, and provide a 'spectral decomposition' of $\hat{f}_{z_0}$: In the interaction picture with respect to the Hamiltonian of the system, they evolve as $\hat{f}^{(\Delta E_j)}(t) = \hat{f}^{(\Delta E_j)}\exp(-i\Delta E_j t/\hbar)$.

Let ΔE be a typical level spacing between physically relevant states such that $\Delta E_j \geq \Delta E$, then for $\kappa \ll \Delta E$ the effects of the off-diagonal elements with $\Delta E_j \neq 0$ will be strongly suppressed. Following the derivation in Appendix B, we arrive at the SME for the conditional density matrix

$$d\tilde{\rho}_c = -i[\hat{H}, \tilde{\rho}_c]dt + \gamma\mathcal{D}[\hat{f}^{(0)}]\tilde{\rho}_c dt + \sqrt{\gamma}\mathcal{H}[\hat{f}^{(0)}]\tilde{\rho}_c dW(t)$$
$$+ \sum_{\Delta E_j \neq 0}\gamma_j\mathcal{D}[\hat{f}^{(\Delta E_j)}]\tilde{\rho}_c dt, \quad \text{(C2)}$$

where we have assumed a resonant cavity driving, $\delta = 0$, and the homodyne angle $\phi = -\pi/2$. In Eq. (C2), $\hat{f}^{(0)} = \hat{f}^{(\Delta E_j=0)} = \sum_{\vec{\nu}} f_{\vec{\nu}\vec{\nu}}|\vec{\nu}\rangle\langle\vec{\nu}|$ is the QND observable which measures the local density for an arbitrary eigenstate, with a rate $\gamma = [4\mathcal{A}\mathcal{E}/(\hbar\kappa)]^2$. Analogous to the single-particle case [c.f. Eq. (B9)], the last term of Eq. (C2) describes the suppressed dissipation channels, with the rates $\gamma_j = \gamma\sum_{\vec{\nu},\vec{\nu}'}' f_{\vec{\nu}\vec{\nu}'}^2[1 + 4(E_{\vec{\nu}} - E_{\vec{\nu}'})^2/\kappa^2]^{-1}$, where the summation is performed over the states satisfying the constraint $E_{\vec{\nu}} - E_{\vec{\nu}'} = \Delta E_j$. Finally, eliminating the cavity also generates cavity-mediated interactions between particles, which nevertheless can be neglected in the region of interests $\kappa \ll \Delta E$.

The associated expression for the homodyne current reads

$$I(t) = 2\sqrt{\gamma}\text{Tr}[\hat{f}^{(0)}\tilde{\rho}_c(t)] + \xi(t). \quad \text{(C3)}$$

We now apply the above analysis to a simple example of a non-interacting Fermi sea, where the presence of a single impurity causes the Friedel oscillation. Consider N fermions in a one-dimensional box of length $L \gg \sigma$, $-L/2 \leq z \leq L/2$, with a point-like impurity at the origin described by the potential $V_{imp}(z) = U\delta(z)$. Assuming zero boundary conditions at $z = \pm L/2$ and taking the limit $U \rightarrow \infty$ to simplify anlytical expressions, the single-particle wave functions read

$$\psi_n^{(o)}(z) = \sqrt{\frac{2}{L}}\sin\left(\frac{2\pi n}{L}z\right),$$
$$\psi_n^{(e)}(z) = \sqrt{\frac{2}{L}}\sin\left(\frac{2\pi n}{L}|z|\right), \quad \text{(C4)}$$

where $n = 1, 2,\ldots$ for both $\psi_n^{(o)}(z)$ (odd parity) and $\psi_n^{(e)}(z)$ (even parity). The corresponding eigenenergies

are $\epsilon_n^{(o/e)} = [2\pi^2\hbar^2/(mL^2)]n^2$. The particle density for the ground state is (we assume even N for simplicity)

$$
\begin{aligned}
n(z) &= \sum_{n=1}^{N/2}[\psi_n^{(o)}(z)^2 + \psi_n^{(e)}(z)^2] \\
&= n_F + \frac{1}{L}\left\{1 - \frac{\sin[2\pi(N+1)z/L]}{\sin(2\pi z/L)}\right\},
\end{aligned}
\quad\text{(C5)}
$$

where $n_F = N/L$ is the average fermionic density. In the vicinity of the impurity, $|z| \ll L/2\pi$, $n(z)$ has the form of Friedel oscillations,

$$
n(z) \approx n_F - \frac{\sin(2k_F z)}{2\pi z} = n_F\left[1 - \frac{\sin(2k_F z)}{2k_F z}\right], \quad \text{(C6)}
$$

with $k_F = \pi n_F$ the Fermi wave vector, and we omit terms $\sim L^{-1}$. Note that for $z \sim L/2\pi$ the "finite-size" oscillations in $n(z)$, Eq. (C5), have the amplitude $\sim L^{-1}$ that vanishes in the thermodynamic limit with the fixed density n_F, in contrast to the Friedel oscillations Eq. (C6).

For this case it is convenient to classify the many-body states in terms of occupations of single-particle states and to use the language of second quantization. We introduce the destruction (thus the associated creation) operators as $\hat{b}_{n,L(R)} = \frac{1}{\sqrt{2}}\int_{-L/2}^{L/2} dz[\psi_n^{(o)*}(z) \mp \psi_n^{(e)*}(z)]\hat{\psi}(z)$ [with $\hat{\psi}(z)$ the fermi field operator], which correspond to the left(right) single-particle eigenmodes. The focus function $f_{z_0}(\hat{z})$ has zero matrix elements between left and right eigenmodes, $\langle m, L|f_{z_0}(\hat{z})|n, R\rangle = 0$. Using these bases and for simplicity defining the single-particle quantum number $\nu \equiv \{n, L(R)\}$, Eqs. (C2) and (C3) can be expressed explicitly: the QND observable $\hat{f}^{(0)}$ becomes $\hat{f}^{(0)} = \sum_\nu f_{\nu\nu}b_\nu^\dagger b_\nu$ whereas the last term of Eq. (C2) (the suppressed dissipations channels) reads $\sum_{\nu\neq\nu'}\gamma_{\nu\nu'}\mathcal{D}[\hat{b}_\nu^\dagger\hat{b}_{\nu'}]$ with the corresponding rates $\gamma_{\nu\nu'} = \gamma f_{\nu\nu'}^2[1 + 4(\epsilon_\nu - \epsilon_{\nu'})^2/\kappa^2]^{-1}$, where $f_{\nu\nu'} = \langle\nu|f_{z_0}(\hat{z})|\nu'\rangle$ is the single-particle matrix element and $\epsilon_\nu = [2\pi^2\hbar^2/(mL^2)]n^2$. By truncating to a suitable number of fermi orbitals, Eqs. (C2) and (C3) can then be integrated straightforwardly.

To resolve the Friedel oscillations in the scan, their period has to be larger than the focusing region σ, $\pi/k_F > \sigma$. This condition puts an upper bound on the density of fermions and, therefore, on their total number, $N < L/\sigma$, which corresponds to having not more than one fermion per length σ. The gap to the first excited state (the level spacing) in this case can be estimated as $\Delta E \sim \hbar^2/(m\sigma^2)$, and the condition for the non-demolition scan reads $\kappa \leq \hbar^2/(m\sigma^2)$. For the simulation shown in Fig. 4b of the main text, we consider $N = 16$ fermions, scanned by a microscope with resolution $\sigma = 0.01L$ and cavity linewidth $\kappa = 4\pi^2\hbar^2/(mL^2)$. The dimensionless measurement strength is $\gamma T = 400$ with T being the total scanning time. The filter integration time for post-processing is chosen as $\tau = \sigma T/L = 0.01T$.